

potentials. The scattering time is directly measured by monitoring the time evolution of the momentum distribution following a quantum quench. Its behavior is observed over more than three orders of magnitude by controlling the atomic initial momentum and the disorder amplitudes. The measured scattering times are compared to numerical simulations and to theoretical predictions computed in the first-order Born approximation. The latter allows us to identify the weak scattering regime, where a good agreement is observed with the Born predictions, and to study the crossover to the strong scattering regime where significant deviations are reported. Most importantly, we highlight the strong influence of the disorder statistics on this crossover by considering potentials with distinct amplitude distributions, namely attractive and repulsive laser speckle disorder [Fig. 1(a)]. For reference, we complement our analysis by a numerical study of a disordered potential with Gaussian amplitude distribution, a model widely used in the context of condensed matter physics.

First-order Born approximation.— For weak disorder, we can develop an intuitive, physical picture of the scattering time based on the 1st-order Born approximation (referred to as Born approximation in the following) [1, 2]. In this perturbative treatment, τ_s can be interpreted as the finite lifetime of the incoming free state $|\mathbf{k}_i\rangle$, as it is scattered towards a continuum of final momenta $|\mathbf{k}'\rangle$ with $|\mathbf{k}'| = |\mathbf{k}_i|$. The initial momentum distribution therefore decays exponentially in this regime, with the characteristic time τ_s :

$$n(\mathbf{k}_i, t) = n(\mathbf{k}_i, 0) e^{-t/\tau_s}, \quad (1)$$

where t is the propagation time in the disorder. The scattering is only allowed if there exists a spatial frequency component \mathbf{k}_{dis} in the disordered potential that matches the elastic scattering condition $\mathbf{k}_{\text{dis}} = \mathbf{k}' - \mathbf{k}_i$ [Fig. 1(a)]. The weight of scattering in this direction relies uniquely on the spatial frequency distribution of the disorder $\tilde{C}(\mathbf{k}_{\text{dis}})$, i.e., the Fourier transform of the two-point correlation function $C(\Delta\mathbf{r}) = \overline{V(\mathbf{r})V(\mathbf{r} + \Delta\mathbf{r})}$ (where $\overline{\cdots}$ refers to disorder averaging). Using the Fermi golden rule, the Born elastic scattering time τ_s^{Born} is obtained by summing the contributions coming from the scattering in all directions, yielding:

$$\frac{\hbar}{\tau_s^{\text{Born}}} = 2\pi \sum_{\mathbf{k}'} \tilde{C}(\mathbf{k}' - \mathbf{k}_i) \delta[\epsilon_{\mathbf{k}'} - \epsilon_{\mathbf{k}_i}], \quad (2)$$

where $\epsilon_k = \hbar^2 k^2 / 2m$ is the free-state energy, with m the atomic mass.

The correlation length σ of the disorder, i.e., the typical width of $C(\Delta\mathbf{r})$, introduces a characteristic spatial frequency σ^{-1} that defines two scattering regimes. For low initial momentum $k_i \ll \sigma^{-1}$, the disorder contains the spatial frequencies that are necessary to scatter the atoms in all directions and the scattering is isotropic

[see Fig. 1(b)]. In the opposite case of large momentum $k_i \gg \sigma^{-1}$, the disorder's spatial frequencies are too low for satisfying the backward scattering condition ($\mathbf{k}_{\text{dis}} = -2\mathbf{k}_i$) and the scattering is essentially concentrated in the forward direction. As discussed in [20, 25–27], the Born prediction (2) behaves differently in the two regimes: τ_s^{Born} is essentially constant for isotropic scattering while it increases linearly with momentum in the forward case (see dashed lines in Fig. 2 and [29] for further details).

Note that the validity of the Born approximation can be estimated in an intuitive manner. Due to its finite lifetime τ_s^{Born} , the matter wave acquires a finite energy width $\Delta\epsilon = \hbar/\tau_s^{\text{Born}}$ [responsible for the ring's width seen in Fig. 1(b)]. By consistency, $\Delta\epsilon$ should be much smaller than the initial energy $\epsilon_{k_i} \propto k_i^2$, yielding the usual weak scattering criterion $k_i l_s^{\text{Born}} \gg 1$ introduced above (with $l_s^{\text{Born}} \propto k_i \tau_s^{\text{Born}}$). In the following we study experimentally and numerically the validity of this criterion by analyzing scattering times for various potential disorders $V(\mathbf{r})$ and over a large range of initial momentum \mathbf{k}_i , allowing us to investigate the crossover between weak and strong scattering.

Experiment.— Based on Eq. (1), we directly measure τ_s by monitoring the decay of the initial momentum distribution of atoms launched with a well defined initial momentum \mathbf{k}_i into a disordered potential $V(\mathbf{r})$ [24]. The experimental set-up is similar to the one described in Refs. [30, 31]. It relies on the production of a quasi non-interacting cloud of 10^5 ^{87}Rb atoms in a $F = 2$, $m_F = -2$ Zeeman sublevel, suspended against gravity by a magnetic field gradient. A delta-kick cooling sequence leads to an ultra-narrow momentum spread $\Delta k = 0.15 \mu\text{m}^{-1}$ ($T \sim 150$ pK). A mean initial momentum \mathbf{k}_i , ranging from $k_i = 1 \mu\text{m}^{-1}$ to $k_i = 20 \mu\text{m}^{-1}$ along the y axis, is then given to the atoms by pulsing an external magnetic gradient for a tunable duration.

A quasi-2D disordered potential in the $(y-z)$ plane is created by laser speckle field [32, 33], realized by passing a laser beam along the x axis through a rough plate and focusing it on the atoms [29]. The wavelength of the laser is red- or blue-detuned with respect to the atomic transition (D_2 line of ^{87}Rb around 780 nm) in order to create either an attractive or a repulsive disordered potential [see Fig. 1(a)]. The detuning small enough ($\Delta \sim 1$ THz), both disorders have the same spatial correlation function, with a measured correlation length $\sigma = 0.50(1) \mu\text{m}$ (radius at $1/e$). However, they differ by their probability distribution $P(V)$, both exhibiting the asymmetrical exponential distribution of laser speckle fields [33], but with opposite signs (see inset of Fig. 3). It yields $P(V) = |V_R|^{-1} e^{-V/V_R} \cdot \Theta(V/V_R)$, with Θ the step function. Here V_R is the averaged amplitude (negative for attractive and positive for repulsive laser speckle), while the rms disorder amplitude, i.e., the quantity that characterizes the disorder strength, is the absolute value

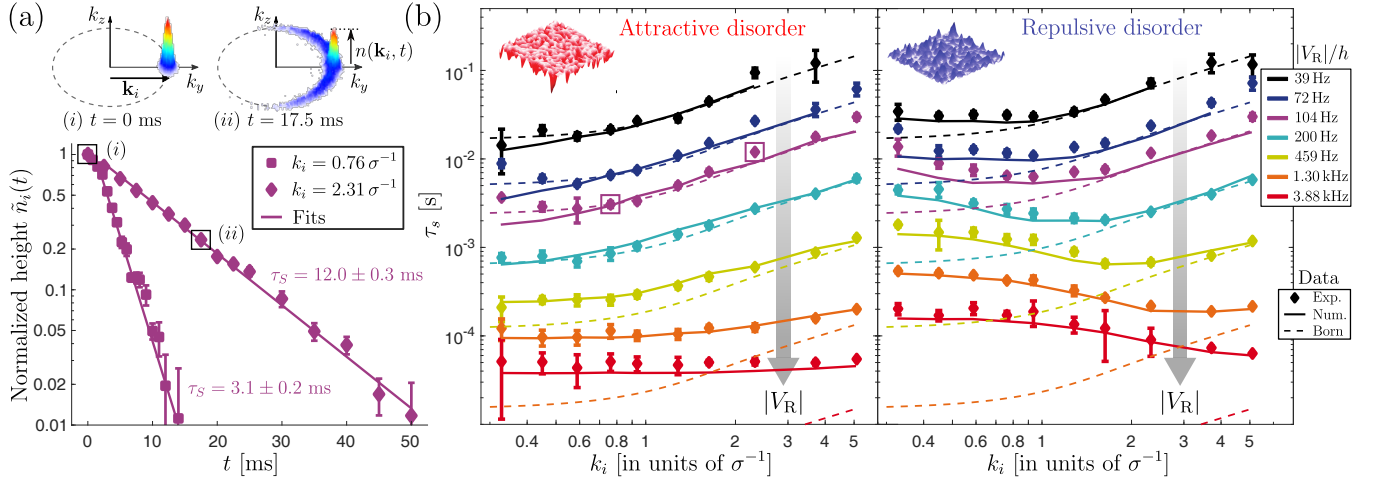


FIG. 2. **Measurements of the elastic scattering time τ_s .** (a) Measurement procedure. The momentum distributions $n(\mathbf{k}, t)$ are observed for different propagation times t in the disorder, here shown for the parameters $V_R/h = -104$ Hz (attractive case) and $k_i = 2.31 \sigma^{-1}$. The normalized height $\tilde{n}_i(t)$ is determined from $n(\mathbf{k}, t)$ by a Gaussian fit of the radially integrated angular profile [29]. When plotted as a function of the time t , it shows an exponential decay from which is extracted τ_s , as illustrated for two different initial momentum $k_i = 0.76 \sigma^{-1}$ and $k_i = 2.31 \sigma^{-1}$, still at $V_R/h = -104$ Hz. (b) Experimental (points) and numerical (solid lines) measurements of τ_s as function of the initial momentum k_i for different values of the disorder amplitude $|V_R|$, in the cases of an attractive disorder (left panel) and a repulsive disorder (right panel). The initial momenta are shown in units of the characteristic frequency σ^{-1} of the disorder. Born predictions τ_s^{Born} are indicated by dashed lines. Note that the curves are just shifted down for the various disorder amplitudes due to the scaling $\tau_s^{\text{Born}} \propto 1/|V_R|^2$ (see text).

$|V_R|$. When varying the laser power and detuning, $|V_R|/h$ ranges from 39 Hz to 3.88 kHz.

The experimental sequence starts with the preparation of an atomic cloud with momentum \mathbf{k}_i . At $t = 0$ we rapidly switch on the disorder potential $V(\mathbf{r})$, performing a quantum quench of the system. After a time evolution t , the disorder is switched off and we record the momentum distribution $n(\mathbf{k}, t)$ by fluorescence imaging after a long time of flight. Thanks to gravity compensation, up to 300 ms can be achieved, corresponding to a momentum resolution $\Delta k_{\text{res}} = 0.2 \mu\text{m}^{-1}$ [34]. From these images we extract the evolution of the initial momentum distribution $n(\mathbf{k}_i, t)$, as shown in Fig. 2(a) [29]. At low disorder strength $|V_R|$, an exponential decay is observed for almost two orders of magnitude and a fit yields the experimental value of τ_s [refer to Eq. (1)]. Such exponential decay is expected to persist at larger disorder amplitudes, except if one drives the system to the very strong scattering regime (see e.g. [35]). However, no significant departure from an exponential decay was observed in our experiment and all the recorded decays could be fitted by an exponential function.

General results. — Figure 2(b) shows the measured values of the elastic scattering time τ_s for both the attractive and repulsive laser speckle disorder cases. The large set of disorder amplitude and initial momenta allows us to observe variations of τ_s from 40 μs to 100 ms. These observations are compared to 2D numerical calculations (solid lines) [29], with a remarkable agreement over the very broad data range, confirming the quasi-2D charac-

ter of our configuration. Deviations are nevertheless observed in a small zone (very low momenta and disorder amplitudes, upper left part on the graphs) and may be attributed to technical difficulties to precisely measure τ_s in this regime due to the finite momentum resolution Δk_{res} .

The Born prediction (2) is also shown in Fig. 2(b) (dashed lines) [36]. Note that τ_s^{Born} scales with the rms value $|V_R|$ as $1/|V_R|^2$ [29], but does not depend on the specific form of the disorder amplitude distribution $P(V)$. As a consequence, the prediction is strictly identical for both attractive and repulsive speckles, since they possess the same frequency distribution $\tilde{C}(\mathbf{k}_{\text{dis}})$. In general, τ_s^{Born} shows a very good agreement with the data at low scattering strength, i.e., weak $|V_R|$ and large k_i [upper right part on Fig. 2(b)], as expected for this first order perturbative approach. However significant deviations appear already for the lowest disorder amplitude ($|V_R|/h = 39$ Hz, black dots) when considering the low initial momentum range $k_i \lesssim \sigma^{-1}$. As the disorder strength $|V_R|$ increases, the deviations become more pronounced and extend to larger momenta. In strong scattering conditions, the two regimes previously identified (isotropic and forward scattering) are then not relevant anymore. Moreover, large differences are observed between attractive and repulsive disorders, another signature of the complete failure of the Born approximation.

In order to visualize these deviations, we show in Fig. 3 maps of the ratio $\tau_s/\tau_s^{\text{Born}}$ as a function of the parameters k_i and $|V_R|$. The important role of the disorder statistics

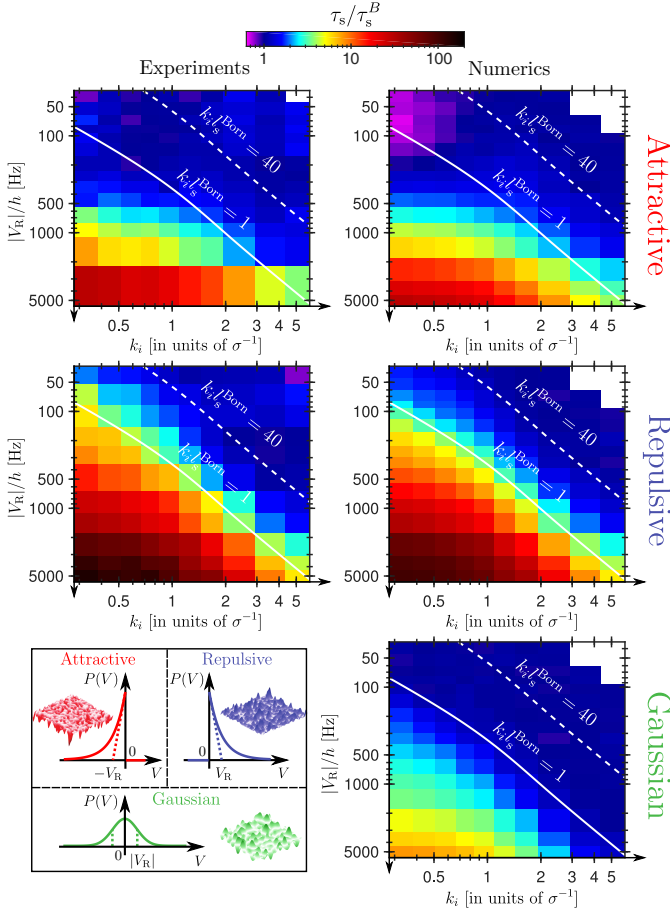


FIG. 3. **Deviations from the Born predictions for different disorder amplitude distributions.** 2D representation (logarithmic color scale) of the ratio $\tau_s/\tau_s^{\text{Born}}$ as a function of $|V_R|$ and k_i for attractive (1st row) and repulsive (2nd row) disordered potentials. Both experimental (left column) and numerical (right column) data are shown. 3rd row: same representation for a Gaussian-distributed disorder (numerical study). The amplitude probability distributions $P(V)$ for the three types of disorders are plotted in the inset.

is further emphasized by numerically extending our analysis to the case of a disorder with a Gaussian amplitude probability distribution $P(V) = (\sqrt{2\pi}V_R)^{-1}e^{-V^2/2V_R^2}$ (inset of Fig. 3), $|V_R|$ being still the rms value. For consistency, the same two-point correlation function $C(\Delta\mathbf{r})$ that characterizes the spatial fluctuations of the potential is chosen to be the same as for the laser speckles considered so far [29].

Weak to strong scattering crossover.— The maps shown in Fig. 3 allow us to investigate the crossover between the weak (Born regime) and strong scattering regimes. Considering first the case of a Gaussian-distributed disorder (3rd row), we observe a striking coincidence between the iso-deviation lines and the dimensionless parameter $k_i l_s^{\text{Born}}$. In particular, the $k_i l_s^{\text{Born}} = 1$ line, i.e. the usual criterion introduced earlier, corresponds to a typical deviation of 25%. Importantly

enough, this observation confirms, in a quantitative manner, the relevance of the criterion $k_i l_s^{\text{Born}} = 1$ to differentiate the weak and strong scattering regimes for this commonly used type of disorder [37].

In contrast, this criterion does not hold for laser speckle disorders, the deviations to the Born prediction being much more pronounced. For instance, the $k_i l_s^{\text{Born}} = 1$ line corresponds now to deviations up to 250% for the attractive case (1st row) and to 400% for the repulsive case (2nd row). As a result, the crossover is significantly shifted towards larger $k_i l_s^{\text{Born}}$ values, i.e. larger momenta and lower disorder amplitudes. More precisely, the same 25% deviation as considered above yields to an effective criterion $k_i l_s^{\text{Born}} = 40$ (white dashed lines).

Beyond the 1st-order Born approximation.— An exhaustive description of the deviations to the Born prediction is beyond the scope of the present letter [38]. It is however possible to get some physical insight by considering two different regimes. First, in the intermediate scattering regime at low momenta and low disorder amplitude (upper left part of the maps in Fig. 3), the deviations can still be understood within perturbative theory [1, 2], but going to higher order corrections [20, 39, 40]. Since the next higher-order term scales as $1/V_R^3$, it is negative for attractive speckle disorder, positive for the repulsive one, but vanishes for Gaussian disorder due to the symmetry of the probability distribution. This explains the important difference between the three types of disorder in this parameter range.

When going to the very strong scattering regime (lower left part of the maps), the perturbative approach completely breaks down. To interpret the data, it is then fruitful to invoke the general concept of spectral functions $A_{\mathbf{k}_i}(E)$, which give the energy probability distribution of the initial state $|\mathbf{k}_i\rangle$ once the disorder is switched on. Their width is indeed inversely proportional to the measured scattering time τ_s [41]. In the strong disorder limit, the spectral functions are known to converge towards the disorder amplitude distribution $P(V)$ [35, 42, 43]. As a result τ_s essentially scales as $1/|V_R|$ in this limit, yielding to values well above the Born prediction (scaling as $1/|V_R|^2$, see above). Such general trend explains the large positive deviations observed in Fig. 3. In this regime, the specific shape of the spectral functions associated to each type of disorder leads however to discrepancies for the measured scattering times [35, 42, 43]. In particular the spectral functions for the repulsive speckle disorder exhibits a narrow peak at low energy [44], which is responsible for the striking increase of the scattering time (almost two orders of magnitude from the Born prediction). In order to support this analysis, we have verified the very good agreement between the present measurements and the width of the spectral functions recently measured for laser speckle disorders in Ref. 43.

Conclusion.— We have investigated, both experimentally and numerically, the elastic scattering time of mat-

ter waves in disordered potentials. The comparison with the Born prediction over a large range of experimental parameters allowed us to study the crossover from the weak to the strong scattering regime. Most importantly, we found that the criterion used to differentiate these regimes strongly depends on the disorder statistics. While the widely used $kl_s = 1$ limit is accurate for the Gaussian-distributed disorder, much stronger deviations are reported (even at moderate disorder strength) for laser speckle cases, an effective criterion being identified around $kl_s = 40$.

Our work motivates further investigations, both on experiments and theory. For the latter, it would be very interesting to go beyond the Born approximation and compare the data to higher order perturbative theories [20, 28, 39, 40], Self-Consistent Born Approximation [21, 23, 45] or semiclassical approaches [35, 42]. On the experimental side, a direct follow-up would be to measure the transport time τ^* [24, 46], another fundamental quantity that characterizes the isotropization of the momentum distribution [1, 2]. In general, future studies of the dynamics of the atomic momentum distribution will allow us to address quantum transport in disordered media in a new way. In addition to the search for direct signatures of single particle localization phenomena [24, 30, 31, 47–49], a strong interest will be to study the thermalization in presence of interactions [50], in connection with the recent concept of many-body localization [51–53].

We would like to thank G. Montambaux, S. Skipetrov, D. Delande, and C. Müller for fruitful discussions and comments. This work was supported by ERC (Advanced Grant “Quantatop”), the Institut Universitaire de France, the Region Ile-de-France in the framework of DIM Nano-K (project QUGASP), the French Ministry of Research and Technology (ANRT, through a DGA grant for J. R. and CIFRE/DGA grant for V. D.), and the EU-H2020 research and innovation program (Grant No. 641122-QUIC and Marie Skłodowska-Curie Grant No. 655933).

* Corresponding author: vincent.josse@institutoptique.fr

- [1] J. Rammer, *Quantum Transport Theory*, Frontiers in Physics (Avalon Publishing, 2004).
- [2] E. Akkermans and G. Montambaux, *Mesoscopic physics of electrons and photons* (Cambridge University Press, 2007).
- [3] M. Monteverde, C. Ojeda-Aristizabal, R. Weil, K. Ben-naceur, M. Ferrier, S. Guéron, C. Glatli, H. Bouchiat, J. N. Fuchs, and D. L. Maslov, Phys. Rev. Lett. **104**, 126801 (2010).
- [4] A. Lagendijk, B. van Tiggelen, and D. S. Wiersma, Physics Today **62**, 24 (2009).
- [5] The transport properties are linked to the transport time τ^* , which is related to the isotropization of the momentum distribution [1, 2].
- [6] H. H. J. M. Niederer, Japanese Journal of Applied Physics **13**, 339 (1974).
- [7] T. Ando, A. B. Fowler, and F. Stern, Rev. Mod. Phys. **54**, 437 (1982).
- [8] U. Bockelmann, G. Abstreiter, G. Weimann, and W. Schlapp, Phys. Rev. B **41**, 7864 (1990).
- [9] J. H. Page, P. Sheng, H. P. Schriemer, I. Jones, X. Jing, and D. A. Weitz, Science **271**, 634 (1996).
- [10] R. Savo, R. Pierrat, U. Najar, R. Carminati, S. Rotter, and S. Gigan, Science **358**, 765 (2017).
- [11] S. L. Jacques, B. Wang, and R. Samatham, Biomed. Opt. Express **3**, 1162 (2012).
- [12] D. Sevrain, M. Dubreuil, A. Leray, C. Odin, and Y. L. Grand, Opt. Express **21**, 25221 (2013).
- [13] C. Martin and A. Ben-Yakar, Journal of Biomedical Optics **21**, 115004 (2016).
- [14] B. Shapiro, Phys. Rev. Lett. **57**, 2168 (1986).
- [15] P. Sebbah, B. Hu, A. Z. Genack, R. Pnini, and B. Shapiro, Phys. Rev. Lett. **88**, 123901 (2002).
- [16] V. Emiliani, F. Intonti, M. Cazayous, D. S. Wiersma, M. Colocci, F. Aliev, and A. Lagendijk, Phys. Rev. Lett. **90**, 250801 (2003).
- [17] D. Anache-Ménier, B. A. van Tiggelen, and L. Margerin, Phys. Rev. Lett. **102**, 248501 (2009).
- [18] A. Obermann, E. Larose, L. Margerin, and V. Rossetto, Geophysical Journal International **197**, 435 (2014).
- [19] W. K. Hildebrand, A. Strybulevych, S. E. Skipetrov, B. A. van Tiggelen, and J. H. Page, Phys. Rev. Lett. **112**, 073902 (2014).
- [20] R. Kuhn, O. Sigwarth, C. Miniatura, D. Delande, and C. Müller, New Journal of Physics **9**, 161 (2007).
- [21] S. E. Skipetrov, A. Minguzzi, B. A. van Tiggelen, and B. Shapiro, Phys. Rev. Lett. **100**, 165301 (2008).
- [22] M. Hartung, T. Wellens, C. A. Müller, K. Richter, and P. Schlagheck, Phys. Rev. Lett. **101**, 020603 (2008).
- [23] A. Yedjour and B. A. van Tiggelen, Eur. Phys. J. D **59**, 249 (2010).
- [24] N. Cherroret, T. Karpiuk, C. A. Müller, B. Grémaud, and C. Miniatura, Phys. Rev. A **85**, 011604 (2012).
- [25] M. Piraud, L. Pezze, and L. Sanchez-Palencia, EPL (Europhysics Letters) **99**, 1 (2012).
- [26] B. Shapiro, Journal of Physics A: Mathematical and Theoretical **45**, 143001 (2012).
- [27] M. Piraud, L. Pezzé, and L. Sanchez-Palencia, New Journal of Physics **15** (2013), 10.1088/1367-2630/15/7/075007.
- [28] M. Piraud, L. Sanchez-Palencia, and B. van Tiggelen, Phys. Rev. A **90**, 063639 (2014).
- [29] See Supplemental Material at [URL will be inserted by publisher] for details on the measurement of the scattering time, the generation and characterization of laser speckle disordered potential, the calculation of the Born predictions and the numerical simulations.
- [30] F. Jendrzejewski, K. Müller, J. Richard, A. Date, T. Plisson, P. Bouyer, A. Aspect, and V. Josse, Phys. Rev. Lett. **109**, 195302 (2012).
- [31] K. Müller, J. Richard, V. V. Volchkov, V. Denechaud, P. Bouyer, A. Aspect, and V. Josse, Phys. Rev. Lett. **114**, 205301 (2015).
- [32] D. Clément, A. F. Varón, J. A. Retter, L. Sanchez-Palencia, A. Aspect, and P. Bouyer, New Journal of Physics **8**, 1 (2006).
- [33] J. W. Goodman, *Speckle phenomena in optics: theory*

and applications (Roberts and Company, 2007).

- [34] It includes the initial momentum spread Δk and the initial size of the cloud of $30\text{ }\mu\text{m}$.
- [35] M. I. Trappe, D. Delande, and C. A. Müller, J. Phys. A **48**, 245102 (2015).
- [36] It corresponds to 2D calculations, which are found in excellent agreement with full 3D calculations [29].
- [37] The criterion $k_i l_s^{\text{Born}} \sim 1$ deviates significantly from the criterion $\Delta = V_R^2 / \epsilon_k E_\sigma \sim 1$ discussed in Ref. [20], with $E_\sigma = \hbar^2 / m \sigma^2$ the correlation energy.
- [38] A detailed analysis is in preparation.
- [39] P. Lugan, A. Aspect, L. Sanchez-Palencia, D. Delande, B. Grémaud, C. A. Müller, and C. Miniatura, Phys. Rev. A **80**, 023605 (2009).
- [40] E. Gurevich and O. Kenneth, Phys. Rev. A **79**, 063617 (2009).
- [41] H. Bruus and K. Flensberg, *Many-Body Quantum Theory in Condensed Matter Physics* (Oxford University Press, Oxford, England, 2004).
- [42] T. Prat, N. Cherroret, and D. Delande, Phys. Rev. A **94**, 022114 (2016).
- [43] V. V. Volchkov, M. Pasek, V. Denechaud, M. Mukhtar, A. Aspect, D. Delande, and V. Josse, Phys. Rev. Lett. **120**, 060404 (2018).
- [44] This peak can be traced to the presence of many bound states, with similar energies, that are supported by the valleys formed around local minima of the potential [35, 42, 43].
- [45] D. Vollhardt and P. Wölfle, Phys. Rev. Lett. **45**, 842 (1980).
- [46] T. Plisson, T. Bourdel, and C. Müller, The European Physical Journal Special Topics **217**, 79 (2013).
- [47] T. Karpiuk, N. Cherroret, K. L. Lee, B. Grémaud, C. A. Müller, and C. Miniatura, Phys. Rev. Lett. **109**, 190601 (2012).
- [48] S. Ghosh, C. Miniatura, N. Cherroret, and D. Delande, Phys. Rev. A **95**, 041602 (2017).
- [49] C. Hainaut, I. Manai, J.-F. Clément, J. C. Garreau, P. Szriftgiser, G. Lemarié, N. Cherroret, D. Delande, and R. Chicireanu, Nature communications **9**, 1382 (2018).
- [50] N. Cherroret, T. Karpiuk, B. Grémaud, and C. Miniatura, Phys. Rev. A **92**, 063614 (2015).
- [51] R. Nandkishore and D. A. Huse, Annual Review of Condensed Matter Physics **6**, 15 (2015).
- [52] M. Schreiber, S. S. Hodgman, P. Bordia, H. P. Lüschen, M. H. Fischer, R. Vosk, E. Altman, U. Schneider, and I. Bloch, Science (2015), 10.1126/science.aaa7432.
- [53] J.-y. Choi, S. Hild, J. Zeiher, P. Schauß, A. Rubio-Abadal, T. Yefsah, V. Khemani, D. A. Huse, I. Bloch, and C. Gross, Science **352**, 1547 (2016).

Supplemental Material: Elastic Scattering Time of Matter-Waves in Disordered Potentials

J  r  mie Richard,¹ Lih-King Lim,^{2,1} Vincent Denechaud,^{1,3} Valentin V. Volchkov,^{1,4}
Baptiste Lecoutre,¹ Musawwadah Mukhtar,¹ Fred Jendrzejewski,^{1,5} Alain
Aspect,¹ Adrien Signoles,¹ Laurent Sanchez-Palencia,⁶ and Vincent Josse^{1,*}

¹Laboratoire Charles Fabry, Institut d'Optique, CNRS, Université Paris-Saclay, 91127 Palaiseau cedex, France

²*Zhejiang Institute of Modern Physics, Zhejiang University, Hangzhou 310027, P. R. China*

³SAFRAN Sensing Solutions, Safran Tech, Rue des Jeunes Bois,
Châteaufort CS 80112, 78772 Magny-les-Hameaux, France

⁴Max-Planck-Institute for Intelligent Systems, Max-Plack-Ring, 4, 72076 Tübingen, Germany

⁵Heidelberg University, Kirchhoff-Institut für Physik,
Im Neuenheimer Feld 227, 69120 Heidelberg, Germany

⁶CPHT, Ecole Polytechnique, CNRS, Université Paris-Saclay, Route de Saclay, 91128 Palaiseau, France

We describe here the methods (i) to extract the scattering time from the measurement, (ii) to generate and characterize the laser speckle field, (iii) to calculate the Born prediction adapted to our configuration and (iv) to perform the numerical simulations to estimate the scattering times.

EXTRACTION OF THE SCATTERING TIME τ_s

The measurement of the elastic scattering time τ_s is based on the decay of the initial momentum distribution $n(\mathbf{k}_i, t)$, as illustrated in Fig. 1 for the parameters $k_i = 2.31\sigma^{-1}$ and $V_R/h = -104\text{Hz}$ (same as in Fig.2(a) on the main text).

The determination of τ_s is performed in three steps. First, we determine the angular profile $n(\theta, t)$ by radially integrating the momentum distribution $n(\mathbf{k}, t)$ in the (k_y, k_z) plane, $\theta = 0$ corresponding to the initial direction [Fig. 1(a)]. The lower and upper integration limits correspond to twice the radial width of the initial momentum distribution. The reduced angular profile $\tilde{n}(\theta, t) = n(\theta, t)/n(0, 0)$ is obtained by normalizing this profile by its initial value at time $t = 0$ and $\theta = 0$. A typical angular profile $\tilde{n}(\theta, t)$ for $t = 17.5$ ms is plotted on Fig. 1(b) (blue line). The general shape results from the sum of two contributions: a narrow peak $\tilde{n}_i(\theta, t)$ that corresponds to the unscattered initial distribution and a broad background $\tilde{n}_b(\theta, t)$. The latter corresponds to the scattered atoms to direction \mathbf{k}' and builds up progressively on time.

In a second step, the normalized height $\tilde{n}_i(t) = \tilde{n}_i(0, t)$ of the initial distribution is extracted by adjusting the bi-modal distribution by the sum of a narrow Gaussian peak accounting for $\tilde{n}_i(\theta, t)$ [1] and a broad Gaussian peak accounting for the background $\tilde{n}_b(\theta, t)$ [red solid line in Fig.1(b)]. Error bars of $\tilde{n}_i(t)$ represent one standard deviations and are estimated from the noise on the experimental data and the deviation of the model.

To finally extract τ_s , the decay of $\tilde{n}_i(t)$ is plotted in a semi-logarithmic scale [dots in Fig. 1(c)] and then adjusted by a pure exponential law of typical time τ_s .

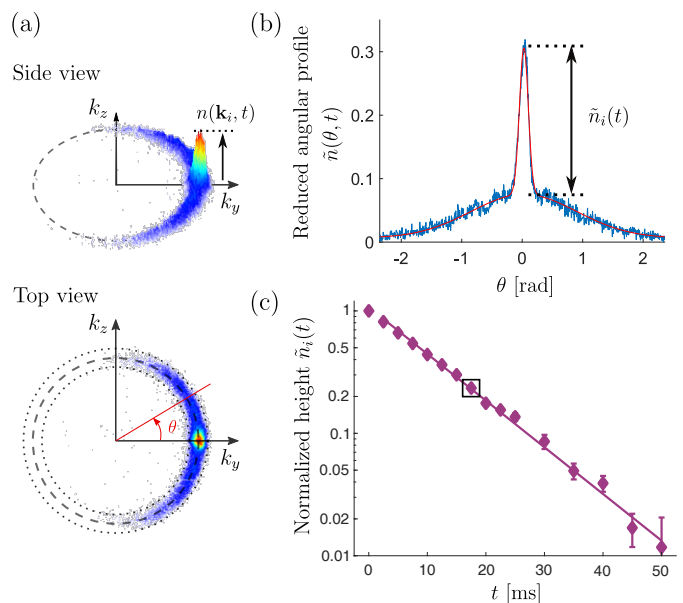


FIG. 1. Measurement protocol of the scattering time τ_s . The procedure is illustrated for the same parameters than in Fig. 2(a) of the main text, i.e., $k_i = 2.31\sigma^{-1}$ and $V_R = -104$ Hz. (a) Observed momentum distribution $n(\mathbf{k}, t)$ after a propagation time $t = 17.5$ ms in the disorder (top: side view; bottom: top view). The angular profile is obtained by radially integrating around the initial peak (between the two dotted lines). (b) The reduced angular profile $\tilde{n}(\theta, t)$ (blue line) is adjusted by the sum of a narrow and a broad Gaussian peak, both centered around $\theta = 0$ (red line). The amplitude of the narrow peak is used to extract the normalized height $\tilde{n}_i(t)$. (c) The normalized height $\tilde{n}_i(t)$ is plotted as a function of the propagation time t . The experimental points are fitted by an exponential function of the form e^{-t/τ_s} . Here we find $\tau_s = 12.0(3)$ ms.

LASER SPECKLE DISORDERED POTENTIAL

Quasi-2D laser speckle field generation

The laser speckle field is created by passing a laser beam of wavelength $\lambda \sim 780$ nm through a diffusive plate, the configuration being identical as the one described in Ref. [2]. As illustrated in Fig. 2(a), the incoming wave that illuminates the diffusive plate is converging at the position $d = 15.2(5)$ mm that coincides with the position of the atoms. The intensity profile of the illumination on the diffusive plate is a Gaussian shape, of waist $w = 9(1)$ mm (radius at $1/e^2$), truncated by a circular diaphragm of diameter $D = 20.3(1)$ mm. This diaphragm sets the maximal numerical aperture to $\text{NA} = \sin(\theta_{\max}) = 0.55(2)$.

In this configuration a so-called Fourier speckle pattern is formed around the position of the atoms. In order to characterize it, the random intensity pattern was recorded at the position of the atoms with an high-resolution optical microscope, see Fig. 2(b). As can be seen, the laser speckle field is very elongated along the propagation axis (x direction), resulting in a quasi-2D potential.

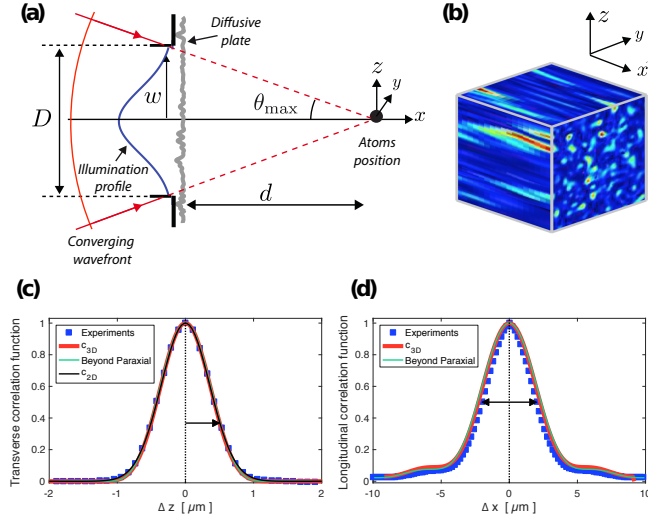


FIG. 2. Laser speckle characterization. (a) Schematic representation of the experimental configuration used for the speckle generation, with $\text{NA} = \sin(\theta_{\max}) = 0.55(2)$. (b) 3D representation of the experimental laser speckle field. (c) Transverse correlation function along the z direction (same along y). Blue squares: experimental measurement c_{exp} from the recorded intensity pattern. Black solid line: transverse Gaussian fit c_{2D} , yielding $\sigma = 0.50(1)\mu\text{m}$ ($1/e$ radius). Red solid line: effective paraxial calculations c_{3D} (see text). Green solid line: beyond paraxial calculations, as done in Ref. 2. This line is barely visible due to superposition with the effective paraxial model. (d) Longitudinal correlation functions with the same legend as in (c). The measured width is $\sigma_{\parallel} = 4.1(1)\mu\text{m}$ (FWHM).

Spatial statistical properties: measurement of the auto-correlation function

The normalized two-point correlation function of the laser speckle field,

$$c_{\text{exp}}(\Delta\mathbf{r}) = \frac{\langle \delta I(\mathbf{r}) \delta I(\mathbf{r} + \Delta\mathbf{r}) \rangle}{\langle \delta I^2 \rangle} \quad \text{with } \delta I = I - \langle I \rangle, \quad (1)$$

is directly calculated from the recorded spatial pattern shown in Fig. 2(b). The resulting transverse and longitudinal correlation functions are respectively shown as blue squares in Fig. 2(c) and (d).

In the transverse plane, the shape is found to be very close to a Gaussian. A fit of the form (solid black line):

$$c_{2D}(\Delta\mathbf{r}_{\perp}) = e^{-\Delta\mathbf{r}_{\perp}^2/\sigma^2}, \quad (2)$$

realized either along the y or z axis, yields $\sigma = 0.50(1)\mu\text{m}$ ($1/e$ radius).

The laser speckle field being very elongated, the correlation function has a much larger width in the longitudinal direction x . It is characterized by the FWHM $\sigma_{\parallel} = 4.1(1)\mu\text{m}$ [see Fig. 2(d)].

Modeling the laser speckle field

Due to the large numerical aperture $\text{NA} = \sin(\theta_{\max}) = 0.55(2)$, the precise modeling of the speckle field requires in principle to go beyond the paraxial approximation. A theoretical model (not detailed here) was thus used in Ref. 2 to reproduce the measured correlation functions, see green solid lines in Fig. 2(c) and (d).

However this theoretical model is quite heavy to handle, especially in view of the determination of the 3D spatial frequency distribution $\tilde{C}(\mathbf{k}_{\text{dis}})$, a key quantity to calculate the Born prediction. Thus, we developed a simpler model, based on the paraxial approximation but including a global geometrical factor x_{scale} to tune the numerical aperture. In this effective paraxial model, the correlation function can be calculated using Fourier Transform (FT) [3]:

$$c_{3D}(\Delta\mathbf{r}_{\perp}, \Delta x) \propto \left| \text{FT} \left[t(\mathbf{R}_{\perp}) I_{\text{inc}}(\mathbf{R}_{\perp}) e^{-i\pi \frac{R_{\perp}^2 \Delta x}{\lambda d}} \right] \frac{\Delta\mathbf{r}_{\perp}}{\lambda d} \right|^2, \quad (3)$$

where $\text{FT}[f(x)]_u = \int_{-\infty}^{+\infty} dx f(x) e^{-2i\pi ux}$. Here $t = \text{disc}[R_{\perp}/(D_{\text{eff}})]$ represent the transmission of a circular diaphragm of diameter $D_{\text{eff}} = x_{\text{scale}} D$, and $I_{\text{inc}} = e^{-2R_{\perp}^2/(w_{\text{eff}})^2}$ is the Gaussian illumination profile on the diffuser, with effective waist $w_{\text{eff}} = x_{\text{scale}} w$.

Setting $x_{\text{scale}} = 0.875(5)$ (resulting in an effective maximal numerical aperture $\text{NA}_{\text{eff}} = 0.5$), the calculated correlation function $c_{3D}(\Delta\mathbf{r})$ matches also very well with the measurements, both on the transverse and longitudinal directions [see red solid lines in Fig. 2(c) and (d)].

Thus, we used this effective paraxial model to calculate the Born prediction for our specific disorder configuration (see below).

Calibration of the disorder amplitude V_R

In practice, the disorder amplitude V_R can be calibrated by combining photometric measurements and calculation of the atomic polarizability [4]. However it is known that such method leads to systematic uncertainties, typically around a few tens of percents (see e.g. Refs. 2 and 5).

Here, we used the excellent agreement between the experimental determination of τ_s and the numerical simulations [see Fig. 2(b) of the main text] to precisely determine the disorder amplitude by applying an overall correction α on the photometric measurement. In practice, the correction factor is calculated by minimizing the differences between the experiments and numerics for the particular momenta $k_i = 0.74 \sigma^{-1}$, leading to $\alpha = 1.29(2)$. We mainly attribute this correction to the difficulty to estimate precisely the extension of the speckle field at the position of the atoms.

FIRST ORDER BORN APPROXIMATION

Rescaled scattering times $\tilde{\tau}_s^{\text{Born}}$

An important feature of the Born prediction is the simple scaling $\tau_s^{\text{Born}} \propto 1/|V_R|^2$ with the disorder amplitude. Indeed, the spatial frequency distribution of the disorder can be written in the form $\tilde{C}(\mathbf{k}_{\text{dis}}) = |V_R|^2 \tilde{c}(\mathbf{k}_{\text{dis}})$, where $\tilde{c}(\mathbf{k}_{\text{dis}})$ is the Fourier transform of the normalized correlation function $c(\Delta\mathbf{r})$ [as in Eq. (1) above]. The Born prediction [see Eq. (2) of the main text] can then be rewritten in the form:

$$\tau_s^{\text{Born}}(\mathbf{k}_i, V_R) = \frac{\hbar E_R}{\pi V_R^2} \cdot \tilde{\tau}_s^{\text{Born}}(\mathbf{k}_i) \quad (4)$$

where $E_R = \hbar^2/m\sigma^2$ is the so-called correlation energy and $\tilde{\tau}_s^{\text{Born}}$ is the rescaled scattering time that gives the dependence with the momentum \mathbf{k}_i . Its expression relies on the integration of the normalized spatial frequency distribution $\tilde{c}(\mathbf{k}_{\text{dis}}) = \tilde{c}(\mathbf{k}' - \mathbf{k}_i)$ over the elastic scattering sphere ($|\mathbf{k}'| = |\mathbf{k}_i|$) [6, 7]:

$$\tilde{\tau}_s^{\text{Born}}(\mathbf{k}_i) = \frac{4\pi^3\sigma^2}{|k_i| \int d\Omega_{\mathbf{k}'} \tilde{c}(\mathbf{k}' - \mathbf{k}_i)}, \quad (5)$$

3D Born prediction $\tilde{\tau}_{s,3D}^{\text{Born}}$

The rescaled Born prediction $\tilde{\tau}_{s,3D}^{\text{Born}}$ corresponding to our experimental configuration is shown in Fig. 3. As

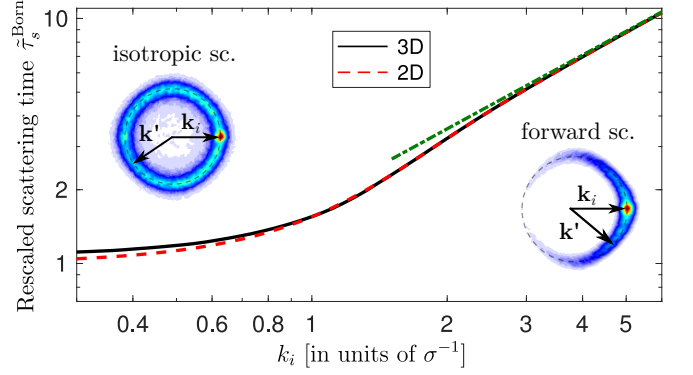


FIG. 3. **Rescaled Born prediction $\tilde{\tau}_s^{\text{Born}}$.** Black solid line: 3D Born prediction $\tilde{\tau}_{s,3D}^{\text{Born}}$ using the correlation $c_{3D}(\Delta\mathbf{r})$ given by Eq. (3) (effective paraxial model). Red dashed line: 2D Born prediction $\tilde{\tau}_{s,2D}^{\text{Born}}$ for a transverse Gaussian correlation of size σ ($1/e$ radius). Green dash-dotted line: asymptotic behavior at large momentum $\tilde{\tau}_s^{\text{Born}} \sim \sqrt{\pi}k_i\sigma$. Illustrations of the momentum distribution in the isotropic ($k_i \ll \sigma^{-1}$) and forward scattering ($k_i \gg \sigma^{-1}$) regimes are the same as in Fig. (1) of the main text.

said above, this calculation uses the effective paraxial model c_{3D} given by Eq. (3) to reproduce the measured two-point correlation function.

Although the configuration is slightly different, the results discussed in Refs. 8 and 9 for the case of a pure Gaussian illumination still hold for our case [10]. First, $\tilde{\tau}_{s,3D}^{\text{Born}}$ increases linearly with the momentum as $\sqrt{\pi}k_i\sigma$ in the large momentum limit ($k_i \gg \sigma^{-1}$), see dash-dotted green line in Fig. 3. This behavior is generic for matter wave and does not depend on the dimension. Second, $\tilde{\tau}_{s,3D}^{\text{Born}}$ tends towards a constant in the low momentum limit ($k_i \ll \sigma^{-1}$). This behavior is specific to the laser speckle disordered potential [11]: it results from the absence of white noise limit due to the infinite correlation range in the longitudinal direction [3].

Comparison with 2D prediction $\tilde{\tau}_{s,2D}^{\text{Born}}$

The very elongated nature of the laser speckle field, having an infinite correlation range along the longitudinal direction, strongly suggests that our experiment can be described by a pure two-dimensional system. This is confirmed by the excellent agreement between the full 3D calculation $\tilde{\tau}_{s,3D}^{\text{Born}}$ and the Born prediction $\tilde{\tau}_{s,2D}^{\text{Born}}$ for a 2D disordered potential having a Gaussian correlation of size σ ($1/e$ radius). In the latter case, one has [9, 12]:

$$\tilde{\tau}_{s,2D}^{\text{Born}}(\mathbf{k}_i) = e^{k_i^2\sigma^2/2}/I_0(k_i^2\sigma^2/2), \quad (6)$$

where I_0 is the zero-order modified Bessel function. $\tilde{\tau}_{s,2D}^{\text{Born}}$ tends towards 1 for low initial momentum ($k_i \ll \sigma^{-1}$) and, as expected, increases in the same way as the 3D case at large momentum ($\tau_s^{\text{Born}} \sim \sqrt{\pi}k_i\sigma$ for $k_i \gg \sigma^{-1}$).

NUMERICAL SIMULATIONS

The numerical calculations are performed by solving the Schrödinger equation for a particle of mass m in a 2D disordered potential $V(\mathbf{r})$. The initial state is a Gaussian wave packet of central momentum k_i and negligible momentum spread Δk [13]. The scattering time τ_s is extracted from the decay of the initial momentum distribution in the same way than for the experimental data (see Fig. 1). The simulations are averaged over 14 different disorder realizations, which is found sufficient to achieve convergence.

To generate the disordered potential, we first calculate the field resulting from the convolution of a spatially uncorrelated complex random field, whose real and imaginary parts are independent Gaussian random variables, with a Gaussian profile accounting for the spatial correlations. The Gaussian-distributed potential is obtained by considering the real part of this field, leading to a Gaussian amplitude probability distribution. Instead, the laser speckle disordered potentials are obtained by considering the intensity (modulus square) of the result-

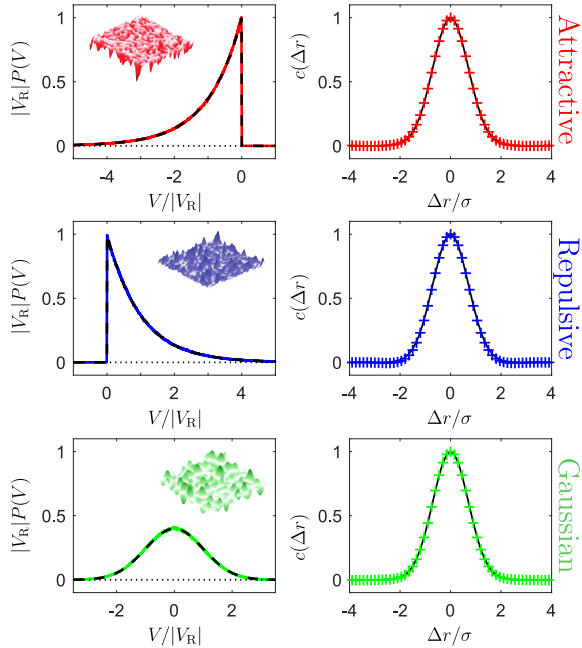


FIG. 4. **Numerically generated disorders.** The amplitude probability distribution $P(V)$ (left column) and the normalized correlation function $c(\Delta r)$ (right column) are shown for attractive (first row), repulsive (second row) and Gaussian-distributed (third row) disordered potentials. The amplitude probability distributions are in perfect agreement with the theoretical functions (black dashed lines), namely an exponential function for the attractive and repulsive disorders and a Gaussian function for the Gaussian disorder. The three disorders exhibit the same correlation function, which corresponds to a Gaussian function of size σ ($1/e$ radius).

ing field [3], with a negative (resp. positive) sign for the attractive (resp. repulsive) disorder.

In each case, we adjust the amplitude of the complex random field for the rms value of the probability distribution to be V_R . It yields $P(V) = |V_R|^{-1} e^{-V/V_R} \cdot \Theta(V/V_R)$, with Θ the step function, for the attractive and repulsive laser speckle fields (first and second rows in Fig. 4), and $P(V) = (\sqrt{2\pi}V_R)^{-1} e^{-V^2/2V_R^2}$ for the Gaussian-distributed disorder (3rd row). In the same way, the spatial width of the Gaussian profile is adjusted in each case for the two-point correlation function of the disorder to be a Gaussian of size σ ($1/e$ radius), i.e., $c(\Delta r) = e^{-\Delta r^2/\sigma^2}$.

* Corresponding author: vincent.josse@institutoptique.fr

- [1] The initial momentum is not an inverted parabola — which is expected for a Bose Einstein condensate in the Thomas Fermi regime — but merely resembles to a Gaussian once the delta-kick cooling technique has been applied.
- [2] V. V. Volchkov, M. Pasek, V. Denechaud, M. Mukhtar, A. Aspect, D. Delande, and V. Josse, Phys. Rev. Lett. **120**, 060404 (2018).
- [3] J. W. Goodman, *Speckle phenomena in optics: theory and applications* (Roberts and Company, 2007).
- [4] D. Clément, A. F. Varón, J. A. Retter, L. Sanchez-Palencia, A. Aspect, and P. Bouyer, New Journal of Physics **8**, 1 (2006).
- [5] G. Semeghini, M. Landini, P. Castilho, S. Roy, G. Spagnolli, A. Trenkwalder, M. Fattori, M. Inguscio, and G. Modugno, Nat. Phys. **11**, 554 (2015).
- [6] J. Rammer, *Quantum Transport Theory*, Frontiers in Physics (Avalon Publishing, 2004).
- [7] E. Akkermans and G. Montambaux, *Mesoscopic physics of electrons and photons* (Cambridge University Press, 2007).
- [8] M. Piraud, L. Pezze, and L. Sanchez-Palencia, EPL (Europhysics Letters) **99**, 1 (2012).
- [9] M. Piraud, L. Pezzé, and L. Sanchez-Palencia, New Journal of Physics **15** (2013), 10.1088/1367-2630/15/7/075007.
- [10] In the case of a pure Gaussian illumination, i.e., for $D \rightarrow \infty$, the longitudinal correlation has a pure Lorentzian shape, and the 3D two-point correlation function reads:

$$c_{3D, \text{Gauss}} = \frac{1}{1 + 4\Delta x^2/\sigma_{\parallel, \text{Gauss}}^2} e^{-\frac{\Delta r_{\perp}^2/\sigma^2}{1 + 4\Delta x^2/\sigma_{\parallel, \text{Gauss}}^2}}. \quad (7)$$

with $\sigma_{\parallel, \text{Gauss}} = 4\pi\sigma^2/\lambda$.

- [11] In the case of a white noise limit, i.e., finite correlation range, the scattering time increases as $\propto 1/|k_i|$ in the low momentum limit.
- [12] B. Shapiro, Journal of Physics A: Mathematical and Theoretical **45**, 143001 (2012).
- [13] We have checked that this momentum spread has no influence on the extracted scattering time.